High-Resolution Field-Cycling NMR Studies of a DNA Octamer as a Probe of Phosphodiester Dynamics and Comparison with Computer Simulation†

Mary F. Roberts,‡ Qizhi Cui,§ Christopher J. Turner,|| David A. Case,§ and Alfred G. Redfield*,⊥

Department of Chemistry, Boston College, Chestnut Hill, Massachusetts 02467, Department of Molecular Biology, Scripps Research Institute, La Jolla, California 92037, Francis Bitter Magnet Laboratory, Massachusetts Institute of Technology, Cambridge, Massachusetts 02139, and Department of Biochemistry, Brandeis University, Waltham, Massachusetts 02454

Received November 6, 2003; Revised Manuscript Received February 2, 2004

ABSTRACT: Phosphorus-spin longitudinal relaxation rates of the DNA duplex octamer $[d(GGAATTCC)]_2$ have been measured from 0.1 to 17.6 T by means of conventional and new field-cycling NMR methods. The high-resolution field-cycling method is identical to a conventional relaxation experiment, except that after preparation the sample is moved pneumatically from its usual position at the center of the high-resolution magnet upward to a lower field above its normal position and then returned to the center for readout after it has relaxed for the programmed relaxation delay at the low field. This is the first measurement of all longitudinal relaxation rates R_1 of a nuclear species in a macromolecule over virtually the entire accessible magnetic field range. For detailed analysis, three magnetic field regions can be delineated: (i) dipolar relaxation dominates at fields below 2 T, (ii) chemical shift anisotropy (CSA) relaxation is roughly constant from 2 to 6 T, and (iii) a square-law increasing dependence is seen at fields higher than ∼6 T due to internal motion CSA relaxation. The analysis provides a rotational correlation time ($\tau_r = 4.1 \pm 0.3$ ns) for the duplex at both 1.5 and 0.25 mM concentrations (of duplex) at 22 °C. For comparison, extraction of τ_r in the conventional way from the ratio of T_1/T_2 at 14 T yields 3.2 ns. The τ_r discrepancy disappears when we exclude the contribution of internal motion from the R_1 in the ratio. The low-field dipolar relaxation provides a weighted inverse sixth power sum of the distances from the phosphorus to the protons responsible for relaxation. This average is similar for all phosphates in the octamer and similar to that in previous B-DNA structures (its inverse sixth root is about 2.40 Å for two different concentrations of octamer). The CSA relaxation at intermediate field provides an estimate of the order parameter squared, S_c^2, for each phosphorus. S_c^2 is about 0.7−1, clearly different for different phosphate linkages in the octamer duplex. The increasing R_1 at high fields reflects CSA relaxation due to internal motions, for which a correlation time, τ_{hf}, can be approximately extracted with the aid of additional measurements at 14.0 and 17.6 T. We conclude that τ_{hf} values are relatively large, in the range of about 150 ps. Insight into the motions leading to this correlation time was gained by a 28 ns molecular dynamics simulation of the molecule. S^2 and τ_s (corresponding to τ_{hf}) predicted by this simulation were in good agreement with the experimental values from the field-cycling data. Both the effect of Mg^{2+} on the dynamic parameters extracted from ^{31}P relaxation rates and the field dependence of relaxation rates for several protons of the octamer were measured. High-resolution field cycling opens up the possibility of monitoring residue-specific dipolar interactions and dynamics for the phosphorus nuclei of diverse oligonucleotides.

Determination of the structure and dynamics of DNA oligomers in solution has been a fertile area of NMR research. Oligomers can be constructed with sequences for interaction with specific proteins or to introduce bulges or loops. Understanding the conformational dynamics of these molecules can often provide direct insights for longer DNA chains. A large number of NMR techniques have been developed to assign protons to specific residues, and to measure interresidue interactions, to extract structural constraints (for examples, see refs *1*−*6*).

At the high fields critical for resolution of ^1H and ^{31}P resonances for each nucleotide in most experiments, the ^{31}P nucleus has not been thought to be very informative because its relaxation is dominated by the chemical shift anisotropy (CSA)[1] mechanism. Specific proton−phosphorus NOEs have been unobservable in small macromolecules for a number of reasons. Information on interactions with protons and extraction of order parameters for the phosphorus moieties

† This research has been supported by NIH Grants GM60418 (to M.F.R.), GM45811 (to D.A.C.), and RR0995 (to C.J.T.) and by the Petroleum Research Fund of the American Chemical Society, Grant 36680-AC4 (to A.G.R.). Equipment was developed with support from the NSF Chemical Instruments Program, Grant CHE-0109575.

* To whom correspondence should be addressed. E-mail: redfield@brandeis.edu.

‡ Boston College.

§ Scripps Research Institute.

|| Massachusetts Institute of Technology.

⊥ Brandeis University.

[1] Abbreviations: CSA, chemical shift anisotropy; HEPES, *N*-(2-hydroxyethyl)piperazine-*N*′-2-ethanesulfonic acid; NOE, nuclear Overhauser effect; NVT/NPT, constant volume/pressure, constant temperature ensemble.

10.1021/bi035979q CCC: $27.50
Published on Web 03/02/2004

are thus difficult to obtain with previous high-resolution techniques. The only previous study of this type known to us was by Lane et al. (*7*). A large body of older work, on short unpaired oligonucleotides and on long DNA duplexes, has been reviewed elsewhere (*8*−*10*). Dynamics of small DNA duplexes have been studied using ^{13}C NMR by several groups (for example, see refs *11*−*13*).

High-resolution field cycling has the potential to provide such information for each resolvable phosphorus nucleus. Any conventional longitudinal relaxation experiment can be converted, using our device (*14*), to a field-cycling experiment by replacing the delay, which we will call the "relaxation delay", between preparation and observation of the nuclear spins by a relaxation delay at a very different, usually lower, magnetic field. The pulse sequence must also include fixed delays, before and after the relaxation delay, long enough for the field to be changed from the high observation field (11.7 T in our case) to the low field, and back.

Studies of the field dependence of relaxation rates have a long and fruitful history (*15*−*21*). For studies of macromolecules, the field dependence is often studied conventionally in fixed field using two or more spectrometers (*22*), as we did in the present study at 11.7 T and above. For studies of nuclei such as ^{17}O or deuterons having submillisecond relaxation times, a few laboratories maintain a combination of conventional and/or tunable spectrometers (*23*, *24*) operating down to fields well below 1 T. A large number of very useful field-dependent relaxation studies (*16*−*21*) have been performed using *field-switched* magnets that are usually copper coils without iron cores that must be efficiently cooled to attain the highest possible preparation and readout fields, so far possible only up to 2 T. Such systems are commercially available (STELAR), and they have the advantage that the switching time is much shorter than the shuttling method that we use, permitting measurement of relaxation rates of up to about 10^3 s^{-1} to be measured. Many useful studies of dynamics have been performed with these instruments on macromolecules in solution, including in liquid crystals. Often the fast switching times of these instruments are advantageous. However, direct observation of resolved macromolecule resonances is not possible in the low available fields of switched magnets because of low sensitivity and poor homogeneity. Therefore, application of these instruments to macromolecules has been limited mainly to use of water and other small molecules as reporters of binding sites.

A relatively small number of cycling experiments, including the present one, are based on *field shuttling*, in which the sample or probe is moved from a high-quality observation field and back (*14*, *25*−*30*), allowing relaxation to be measured at the highest possible resolution (thus the term "high-resolution" in our title) and, equally important, with high sensitivity. A serious limitation of these shuttling methods is that 0.05−0.5 s is required to move the sample, or the probe, the required distance, limiting the fastest rates that can be measured. Among the more recent shuttlers, only those described by Wagner et al. (*30*) and Redfield (*14*) were designed for direct observation of complex molecules in solution, and these have many common features. The instrument described by Wagner et al. (*30*) shuttles the sample down into a lower magnetic field produced by an electromagnet, which produces a relatively homogeneous field of up to about 1 T. Our method is a simplification of this strategy in which we eliminate the electromagnet, as did Kerwood and Bolton (*26*), and instead we use the fringe field above the center of the main magnet of a commercial instrument for the lower field. The lower fringe field, and therefore the relaxation time, for this arrangement can vary significantly over the 1.5 cm sample length, but this disadvantage is unimportant for ^{31}P as reported here, whose relaxation rate varies relatively slowly as a function of field. We have described our shuttling device and methods in detail elsewhere (*14*) and will say little about them here.

We have used these methods to measure the dependence of ^{31}P relaxation rates on magnetic field for a self-complementary DNA octamer, $[d(GGAATTCC)]_2$ previously characterized by Connolly and Eckstein (*31*) using ^{17}O-labeling. Analysis of the field dependence of R_1 provides estimates of the overall molecular rotational correlation time τ_r, an effective distance from the phosphorus nucleus to nearby protons, and a CSA order parameter (S_c) for each phosphate.

We also observed an increasing relaxation rate at higher fields that we analyzed to deduce a time scale for high-frequency internal motions that affect all phosphorus nuclei. Such a high-field effect has not been reported in other macromolecules, to our knowledge, with the exception of some studies of phosphates of phospholipids. As a result we performed a computer simulation of the octamer dynamics. Two ranges of correlation times were deduced from the simulation, of which the longer ones were in excellent agreement with our experimental values for the high-frequency internal motions. Measured and predicted CSA order parameters were also in general agreement.

Quantitative conclusions of this type for nucleic acid phosphates in small synthetic oligomer duplexes have not been achieved, to our knowledge, beyond the early study by Lane et al. (*7*). The ability to measure the relaxation rates of all the phosphorus nuclei over the entire field range for one sample in 1 or 2 days is much more informative than relaxation measurements at a few field strengths. A similar analysis for other DNA or RNA oligomers could be a standard technique in characterizing the structure and dynamics of nucleic acids in solution.

MATERIALS AND METHODS

DNA Preparation. The DNA octamer, $[d(GGAATTCC)]_2$, was obtained from Operon and purified by water-saturated butanol extraction (*32*). Low-conductivity D_2O (Wilmad) and H_2O were used throughout, and glassware was acid-washed (*33*). The oligonucleotide was passed through a 10 mL spin column containing Bio-Rad P2 equilibrated in buffer containing NaCl and phosphate (or HEPES where noted) at pH 7, both diluted to give 50 mM for each in the final volume. The solution was repeatedly lyophilized and redissolved in 99.9% D_2O. For final sample preparation, the dried sample was dissolved in 99.9% D_2O and filtered by spinning through Chelex contained in Bio-Rad 0.22 μm spin filters that were preequilibrated with NMR buffer. Single-strand concentrations, estimated from A_{260}, were 3 or 0.5 mM, referred to below as 1.5 or 0.25 mM in duplex. One of the lots of DNA was kindly analyzed by Kim Hamic, Brandeis University,

using denaturing gel electrophoresis chromatography and showed no significant impurity. The ^1H NMR spectra showed resonances consistent with the composition of the duplex. Mg^{2+} was added as aqueous $Mg(NO_3)_2$ (Alpha Puratronic) diluted according to the supplier's assay for Mg^{2+}. Samples were sealed as described (*14*) in 5 mm, or more often 8 mm, diameter 12.5 cm long thin wall NMR tubes (Wilmad) that were acid-washed before use. Sample volumes of about 0.35 or 0.75 mL were required, respectively.

NMR Methods. All lower field data were taken at 22 °C in a Varian Unity Plus spectrometer using standard 5 and 10 mm probes supplied by Varian, coupled to our shuttler device (*14*). For each cycle of the pulse sequence, the ^1H and ^{31}P magnetizations were first purged with two long pulses on each, shifted relatively 90°, and followed by a 2−3 s recovery delay to achieve a reproducible state. Then dual 90° pulses with the first shifted by 0 or 180° between cycles were applied, to reverse or not reverse the ^{31}P magnetization. These pulses were followed by the relaxation delay at low field above the magnet center. The vacuum and pressure values used to move the sample were set at relatively low values so that raising the sample took 160−250 ms and lowering it took about 150 ms. After the sample was returned to the probe center, a free induction decay of ^{31}P at 11.7 T was recorded with proton decoupling. Runs were typically 0.5−6 h (depending on sample concentration and field), each with six to eight programmed delay times. Noncycling relaxation experiments were also carried out at 14.0 T on a Varian INOVA 600 at Brandeis University and at 17.6 T using a custom-built spectrometer at the Francis Bitter Magnet Laboratory. R_2 values were measured at 11.7 and 14.0 T using the CPMG method with a 1 kHz repetition rate. Proton R_1 rates were measured in a nonselective manner using the same nonselective field-cycling methods as for ^{31}P, except that higher pressure and vacuum settings were used to shorten the cycle time.

Measurement of nonselective NOE from protons to ^{31}P was performed by first pulse-purging both proton and phosphorus magnetizations, followed by a 2−3 s delay ending with the pair of pulses to alternately flip, or not flip, all the protons, similar to the methods described above. Then ^{31}P was purged once more, followed immediately by a field cycle to 1.5 T or less with a mix time of 0.1−0.2 s at low field. After the sample was returned to 11.7 T, the phosphorus signal was observed at 11.7 T, with data reversed by 180° in step with the proton pulse phase reversal earlier in the cycle. The mix time was chosen to be long compared to the proton relaxation time, and short compared to the ^{31}P relaxation time, long enough so that the maximum transfer of magnetization from protons would occur and short enough that the resulting magnetization would not be dissipated by phosphorus relaxation.

Data Analysis. Spectra were plotted, and intensities were measured by computer and/or manually (the latter often used with the cycling experiments while the computer analysis was used for fixed field relaxation rates). Calculation of relaxation rates and analysis of their field dependence as described below were performed using KaleidaGraph software.

For ^{31}P nuclei, the field dependence of R_1 was fit to a sum of terms, reflecting the expected dipolar relaxation contribution, R_1(dipolar), and the CSA contribution, R_1(CSA), including the high-frequency internal contribution to CSA relaxation:

$$R_1 = R_1(\text{dipolar}) + R_1(\text{CSA}) \tag{1a}$$

$$R_1(\text{dipolar}) = [R(0)/2\tau_r][0.1J(\omega_H - \omega_P) + 0.3J(\omega_P) + 0.6J(\omega_H + \omega_P)] \tag{1b}$$

$$R_1(\text{CSA}) = C_L\omega_P^2 J(\omega_P) + C_H H^2 \tag{1c}$$

Here $R(0)$ is the relaxation rate at zero field which we estimate from repeated measurements at 0.05−0.1 T; ω_H and ω_P are the proton and ^{31}P gyromagnetic ratios γ_H and γ_P, multiplied by the magnetic field. The function $J(\omega)$ is the Fourier transform of $\exp(-|\tau|/\tau_r)$ and equals the Lorentzian form $2\tau_r/(1 + \omega^2\tau_r^2)$.

The zero-field dipolar relaxation term $R(0)$ primarily reflects the distances from the nearest protons to the phosphorus. If there was only a single proton dominating the dipolar relaxation of the phosphorus, at a distance r_e from it, then this distance would be related to $R(0)$ by

$$r_e^6 = [\tau_r/R(0)](\mu_0/4\pi)^2(h/2\pi)^2\gamma_P^2\gamma_H^2 \tag{2}$$

Here h is Planck's constant, μ_0 is the permittivity of free space, and we are assuming a single rigid structure. In fact, several protons may be close enough to the phosphorus nucleus to contribute to the relaxation rate, and the variable r_e has to be replaced by the inverse of the sixth root of the sum of the inverse of the sixth powers of the distances to all of the protons; other complications (discussed below) arise from internal motion. Since our experiment does not yield these individual distances, we report the distance r_e, defined from our fit by eq 2, and call it the *effective proton distance*.

Since the size of the CSA interaction is known from model solid-state studies, the coefficient C_L provides an estimate of the CSA order parameter S_c^2 for each phosphorus:

$$C_L = (1/15)(1 + \eta^2/3)\sigma^2 S_c^2 \tag{3}$$

where the symbols σ and η are conventionally defined in terms of the principal elements $\delta_x < \delta_y < \delta_z$ of the traceless CSA tensor for the phosphorus nuclei in the octamer: $\sigma = 1.5\delta_z$, and $\eta = (\delta_x - \delta_y)/\delta_z$. Using average consensus values for the elements of the CSA tensor δ (*34*) comparable to the value for diethyl phosphate (*35*), we take $\sigma = 160$ ppm and $\eta = 0.56$ for all seven phosphates and solve eq 3 to obtain the order parameter for each.

The additional term for high-frequency CSA relaxation, which is represented by the last term in eq 1c, is often assumed to be of the same Lorentzian mathematical form as the first, low-frequency, term in that equation, with a short internal correlation time τ_{hf} replacing the overall rotational correlation time τ_r and $(1 - S_c^2)$ replacing S_c^2 (*36*). We neglect the term $\omega_P^2\tau_{hf}^2$ in the denominator, $1 + \omega_P^2\tau_{hf}^2$, of that spectral density. This is justified for the values of τ_{hf} that we will later infer and the values of field H available to us, for which $\omega_P^2\tau_{hf}^2 \ll 1$. We then can make the correspondence

$$C_H = (2/15)\gamma_P^2\sigma^2(1 - S_c^2)\tau_{hf} \tag{4}$$

We use the values of C_H and S_c^2 from the previous analysis to obtain the internal correlation time τ_{hf}. Here the correction for nonaxial symmetry is ignored since it would be similar in size to the correction $(1 - \eta^2/3)$ in eq 3. That term is about 1.08, compared to 1 for no correction, or 8%, and is small compared to probable errors in our estimates of τ_{hf}, which are likely to be 25% or more. The resulting parameter τ_{hf} which we report would be the correlation time of the high-frequency part of the CSA interaction implied by the data, if the autocorrelation function of that part of the CSA was a single exponential and if only the direction of the principal axes of the interaction were to fluctuate during the high-frequency internal motion and not the magnitudes of the instantaneous CSA tensor elements. The latter assumption is a rigid approximation analogous to the usual assumption of a constant internuclear distance during fluctuations of the dipolar interaction. In fact, neither assumption is necessarily correct, but the low-frequency part of the high-field CSA relaxation is still expected to have the square-law dependence, in field, of the last term of eq 1c above. Therefore, we fit to this simple form, and we report values of τ_{hf}, inferred from values of C_H and S_c^2 obtained from the fit and the use of eq 4, as convenient but tentative phenomenological descriptions of the internal motions.

Fitting of data to these expressions was considerably simplified by noting that the dipolar contribution, eq 1b, is negligible above about 4 T, where $\gamma_P^2 H^2 \tau_r^2 \gg 1$, and the first term of eq 1c is nearly a constant, C_L/τ_r, above the same field. Therefore, as a first step, experimental points at fields higher than this were fit to a constant value, for the first term of eq 1c, plus a square-law term for the second term. In the second step the value of $R(0)$ was estimated directly from the relatively large number of data points at 0.1 T and below, leaving only one variable parameter, τ_r, for a computer fit.

For proton R_1 data as a function of field, simple dipolar relaxation was inadequate to fit the observed data, which approached a constant low rate at high field. A good fit of the observed data used a Lorentzian term plus a constant field-independent rate:

$$R_1 = R(0)/(1 + \gamma_H^2 H^2 \tau_H^2) + c \qquad (5)$$

The values of $R(0)$, c, and τ_H were determined by a computer fit of the field-dependent R_1 data. At the lowest field, the large signal-to-noise ratio of the proton signals allows us to take measurements of the long-time tail of the longitudinal relaxation to enable measurement of the highest rates. The upper end of the sample, which experiences the lowest value of the fringe field during the programmed relaxation delay, may have an appreciably shorter relaxation time than the lower end. Thus the lower end may contribute predominately to the signal, and signals from the rest of the sample may decay much more during transit. As a crude compensation for this systematic error, we recalculated the fields at a point one-fourth of the sample's length (3.25 mm) lower than the center of the sample and then used those fields in our analysis.

Proton−Phosphorus NOE. NOE intensities are expressed as the percentage ratio of the NOE signal to the signal for a simple one-dimensional one-pulse phosphorus spectrum obtained with a long recovery delay and corrected for the number of transients in each experiment.

Molecular Dynamics Simulations. The AMBER 7 suite of programs (*37*) together with the Cornell et al. all-atom force field (*38*) were used to build an initial duplex structure for the DNA octamer $[d(GGAATTCC)]_2$ and to run all simulations. The octamer was solvated in a truncated octahedron TIP3P (*39*) water box. The distance between the wall of the box and the closest atom of the solute is 12.0 Å, leading to a system with 3852 water molecules. Counterions (Na^+) were added to maintain electroneutrality of the system. The system was minimized by first 50 steepest descent steps followed by 950 steps using the conjugate gradient method. The particle mesh Ewald (PME) method (*40*) was used to treat long-range electrostatic interactions, and bond lengths involving bonds to hydrogen atoms were constrained by SHAKE (*41*).

For all simulations, a 2 fs time step and 9 Å direct-space nonbonded cutoff were used. During the equilibration period, harmonic restraints with force constants of 10 kcal mol^{-1} $Å^{-2}$ were applied to the DNA atoms, and the system was heated from 100 to 300 K over 25 ps in the canonical ensemble (NVT); this was followed by 25 ps in the isothermal isobaric ensemble (NPT) simulation to adjust the solvent density under 1 atm of pressure. The harmonic restraints were then gradually reduced to zero with four rounds of 25 ps NVT simulations. After an additional 50 ps of equilibration, 28 ns of "production" NVT simulation was obtained, with snapshots collected every 1 ps. The root-mean-square deviation of the structure from an idealized B-form helix remained less than 2 Å throughout the trajectory, with a slight underwinding being seen, typical of DNA simulations using this force field.

The time-correlation function is defined as (*36*)

$$C_{ab}(\tau) = \langle P_2[\mu_a(t)\cdot\mu_b(\tau + t)]\rangle \qquad (6)$$

where the unit vector μ describes the orientation of a selected vector in a reference frame that is rigidly attached to the molecule, P_2 is the second Legendre polynomial, and the angular brackets indicate ensemble average. Here we report autocorrelations ($a = b$) of the vector pointing from each phosphorus atom to the midpoint of atoms O1P and O2P; this is the symmetry axis direction of the ^{31}P CSA tensor if it is approximated as an axial tensor. As discussed above, the phosphorus CSA tensor is probably fairly nonaxial, with an asymmetry parameter η estimated to be about 0.5. Taking this nonaxial character into account would lead to a more complicated analysis, but the general character of the results should be the same as those found here.

The correlation times and order parameters were obtained by fitting the internal time-correlation functions to an "extended" Lipari−Szabo model (*42*):

$$C(\tau) = S^2 + (1 - S_f^2)\exp(-\tau/\tau_f) + (S_f^2 - S^2)\exp(-\tau/\tau_s) \qquad (7)$$

Here S is the general order parameter (reduction of the CSA interaction by both fast and slow internal motional averaging), S_f is the fast order parameter, and τ_s and τ_f are the slow and fast correlation times, respectively. This double exponential fit is necessary to describe the very fast (<10 ps)

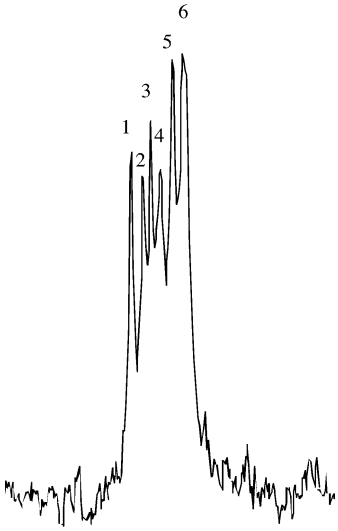

FIGURE 1: ^{31}P NMR spectrum (11.7 T) of the octamer [d(GpGpApApTpTpCpC)]$_2$ with identification of resonances as 1 = CpC, 2 = GpG, 3 = GpA, 4 = TpC, 5 = ApA, and 6 = ApT/TpT. The octamer was 1.5 mM (in duplex) in 50 mM NaCl, 50 mM phosphate, and D_2O, pH 7.

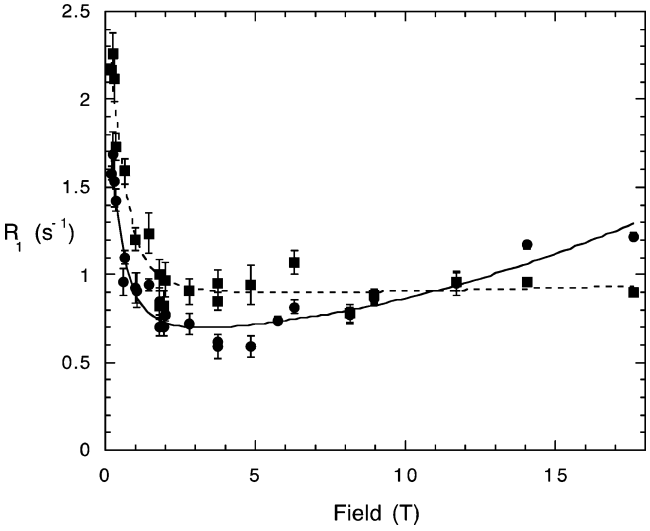

FIGURE 2: Field dependence of R_1 for two of the phosphorus nuclei in the octamer (1.5 mM in duplex): (●) CpC; (■) ApT/TpT. The lines represent the best fits of eq 1 to these data.

vibrational motion, as well as slower (ca. 100 ps) more collective motions. The "slow" mode in these fits corresponds most closely to the "high-frequency" component extracted from the field-dependent curves, as described above.

RESULTS

Field Dependence of ^{31}P R_1 for [d(GGAATTCC)]$_2$ in D_2O. As shown in Figure 1, there are six resolvable resonances for the DNA octamer at 11.7 T and 22 °C, with assignments from Connelly and Eckstein (*31*) listed in the caption. At this field strength, all phosphorus nuclei have nearly the same R_1, 0.97 ± 0.02 s^{-1}. R_2 is less uniform with smaller values for phosphates near the ends of the duplex (R_2 = 11.1 ± 0.1 s^{-1}) and higher rates (14.7 ± 0.2 s^{-1}) for phosphates in the center of the duplex.

High-resolution field cycling, coupled with conventional measurements of R_1 at high fields, can be used to monitor R_1 over a wide range of magnetic fields. Sample data for R_1 from 0.18 to 17.6 T are shown in Figure 2 for the peak assigned to CpC and the combined peak of ApT and TpT. An important feature of the data emerges immediately, namely, that there are fields where rates are different for different resonances. In view of the fact that, in addition to direct overlap of the resonances of ApT and TpT, all of the spectral lines are not well separated, one may ask: to what extent are relaxation differences between different phosphodiesters real, that we report and discuss below? It is likely that relaxation rates that we report are influenced to some extent by spectrally neighboring resonances. Nevertheless, we feel that it is generally true that the larger differences are qualitatively real, because the spectra plotted for different relaxation delays are qualitatively different, to an extent exceeding what might come from noise, for longer delays compared to short ones. We have not attempted to deconvolute our data to reduce possible effects of overlap. This limitation can be considerably removed in cases where 2D observation is easy, as in ^{15}N relaxation measurements in fully ^{15}N-labeled proteins.

The data shown in Figure 2 are typical of all our data and can easily be seen to divide into three regions by magnetic field, corresponding more or less to appearances of different relaxation mechanisms. In the present article, the mechanisms are referred to as dipolar, low-field CSA, and high-field CSA. The three regions are, first, a very low field region with relaxation approaching a definite zero-field value [$R(0)$] and falling off with a roughly Lorentzian behavior (actually the sum of three Lorentzians) around 1−2 T from the *dipolar* interaction between the phosphorus and one or more nearby protons mediated by the overall rotational correlation time of the molecule; second, a roughly constant region above about 2 T due to *low-field CSA* relaxation mediated by the same correlation time in the high-field range, of the expected form $\sigma^2 S_c^2 \gamma_P^2 H^2 \tau_r / [1 + (\gamma_P^2 H^2 \tau_r^2)]$, the low-frequency dip in this prediction being obscured by the rising dipolar relaxation at low fields; and third, a *high-field CSA* region in which the lower end of CSA relaxation mediated by fast ∼0.1 ns internal motion is readily seen, increasing as the square of the field. The rather simple form of the low-field CSA relaxation contribution may be unfamiliar to some readers even though it is derived from the same relaxation theory as the dipolar contribution. The high-field CSA part can be considered as classic short-correlation-time relaxation, but coming from an interaction increasing with field, or equally well as the low end of a curve identical in formal mathematical form to the low-frequency CSA term, but having a different, ∼25-fold shorter correlation time (see the Materials and Methods section above). We assume, mainly for descriptive convenience, that this high-field CSA contribution is $(1 - S_c^2)$ times a Lorentzian expression like the low-field CSA contribution, with a much shorter internal τ_{hf} replacing the overall rotational correlation time τ_r.

The S_c^2 values above are order parameters for the CSA interactions. For the dipolar relaxation we assume that the order parameter (already omitted in eq 1b) equals 1, mainly because we lack any way to determine it. Modification of our analysis, using dipolar order parameters derived from the molecular dynamics simulation, will be discussed later.

An example of the deconvolution into dipolar, CSA, and high-field internal motion CSA contributions is shown in

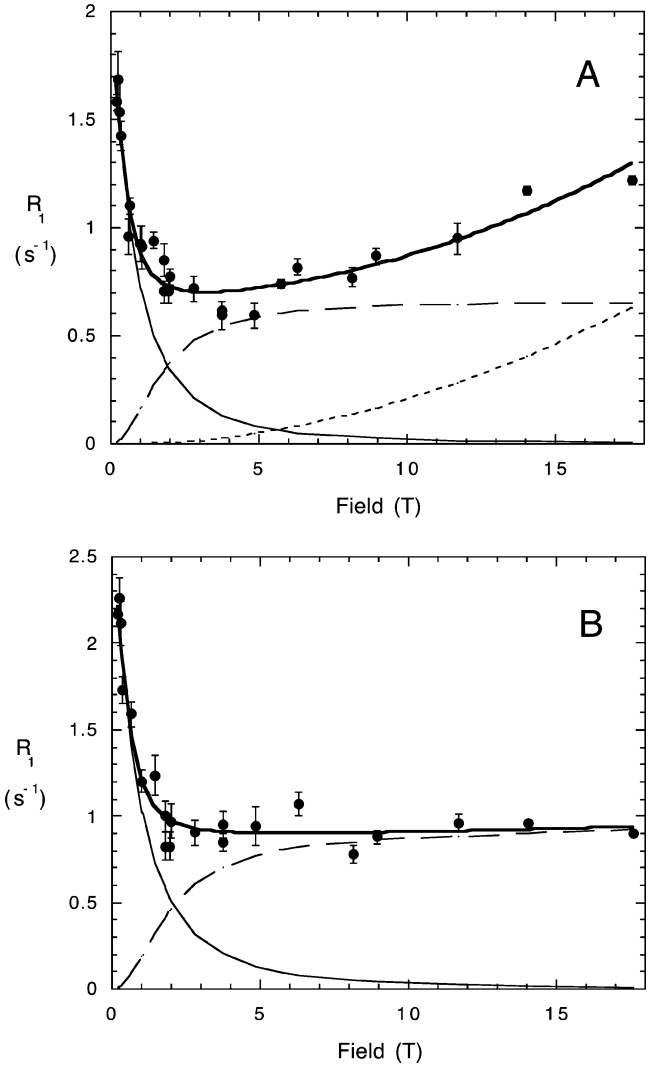

FIGURE 3: (A) Deconvolution of the relaxation behavior of CpC into dipolar (—), low-field CSA (— —), and high-field CSA (- - -) components. (B) Deconvolution of the relaxation behavior of ApT/TpT into dipolar (—) and CSA (— —) components.

Table 1: Correlation Times and Order Parameters for Phosphorus Nuclei in a 1.5 mM (in Duplex) Sample of the DNA Octamer $[d(GGAATTCC)]_2$ Extracted from the Field Dependence of ^{31}P R_1

dinucleoside phosphate	$R(0)$	τ_r (ns)	r_e (Å)	S_c^2	τ_{hf} (ps)
GpG	1.91 ± 0.06	4.7 ± 0.4	2.48	0.87	227
GpA	2.03 ± 0.07	4.4 ± 0.3	2.42	0.76	133
ApA	2.04 ± 0.07	3.5 ± 0.3	2.33	0.68	78
ApT/TpT	2.26 ± 0.12	4.2 ± 0.4	2.36	0.97	129
TpC	1.98 ± 0.08	3.7 ± 0.3	2.36	0.74	82
CpC	1.68 ± 0.07	4.4 ± 0.3	2.50	0.77	227
av	1.98 ± 0.08	4.2 ± 0.2	2.41 ± 0.03	0.80 ± 0.04	146 ± 27

Figure 3A for the CpC resonance. Using this procedure, parameters were extracted for each phosphorus resonance in the 3 mM octamer (1.5 mM duplex) solution (Table 1).

For a molecule containing no large low-frequency internal motion, the rotational correlation time, which is reflected in the width of the low-field portion of the curve, should be the same for all peaks. The average experimental τ_r for this sample was 4.2 ± 0.3 ns, though in some cases the deviation from the average was large (as much as 20%), presumably because the dipolar contribution was more obscured by the CSA contribution.

Table 2: Octamer ^{31}P T_2 Measurements at 11.7 and 14.0 T and Estimation of τ_c from T_1 and T_2 without and with Correction for the High-Field CSA Term

	11.7 T			14.0 T		
dinucleoside phosphate	T_2 (s)	τ_r (ns)	τ_r (ns) corr	T_2 (s)	τ_r (ns)	τ_r (ns) corr
GpG	0.081	3.3	3.7	0.064	3.0	3.5
GpA	0.091	4.3	3.7	0.052	3.4	4.2
ApA	0.068	3.4	3.8	0.054	3.3	3.8
ApT/TpT	0.067	4.3	3.7	0.048	3.6	3.7
TpC	0.069	3.7	3.8	0.055	3.3	3.8
CpC	0.090	3.4	4.0	0.065	2.8	3.7
av		3.8 ± 0.2	3.8 ± 0.1		3.2 ± 0.1	3.8 ± 0.1

The τ_r value provided by analysis of our data at very low field can be compared to the value extracted in the now-traditional way from our measurements of R_1/R_2 at high fixed fields [from $\omega^2\tau_r^2 = 1.5/[(R_1/R_2) - 7/4]$; see ref *43*]. At 11.7 T, this treatment yields $\tau_r = 3.8 \pm 0.2$ ns (Table 2), similar to, but smaller than, that extracted from the field-cycling analysis. A similar calculation of τ_r from R_1/R_2 obtained at 14.0 T gives an average value of 3.2 ± 0.1 ns. The decreased values for τ_r at the higher field from the R_1/R_2 ratios reflect the fact that the internal motion CSA contributes more significantly to R_1 at 14.0 T. Both calculations should be corrected with R_1 given by the observed R_1 minus the contribution due to the internal motion (although the effect at 11.7 T is relatively small). The reduced R_1 leads to an increased τ_r (3.8 ns at both 11.7 and 14.0 T) that is equal, within uncertainty of the error of measurement of R_2 at these high fields, to the values in Table 1.

Our value for the rotational correlation time of 4.2 ns, obtained at 22 °C, can be compared to others recently reported (*11*−*13*), for example, one recently determined by Boisbouvier et al. (*11*), from ^{13}C relaxation for the dodecamer duplex $[d(GCGCAATTGCGC)]_2$ at 35 °C, of approximately 3.2 ns. This value is in good agreement with earlier determinations (*12*, *13*). A rough correction for temperature assuming that the correlation time is proportional to η/T, where η is the viscosity and T is the absolute temperature, as predicted for a rigid sphere of constant size by Stokes' formula, almost removes the difference between measurements, but of course this correction ignores the difference in length between the octamer and the dodecamer. A theoretical correction for the size and shape difference between molecules would presumably lead to the conclusion that our value is somewhat higher than expected from the prior dodecamer estimates, barely outside estimated errors and uncertainties.

Once the correlation time is determined, the zero-field rate $R(0)$ then gives an effective distance between the phosphorus and nearby protons (specifically the sixth root of the r^{-6} sum for all protons). While this distance could vary between different phosphodiesters because of possible small variations in distances to protons for each linkage, it does not vary much outside our experimental error (the range is 2.33−2.50 Å with an average of 2.41 Å). The effective distance of 2.4 Å is in good agreement with the same average (kindly provided by Dr. Jerome Boisbouvier) of 2.23 Å for the NMR structure of the dodecamer (*44*). In that estimate there were approximately equal contributions from one 2′ proton, the 3′ proton, and both 5′ protons, all around 2.9 Å from the

phosphates, and we cannot say which protons of these four contribute most strongly, without further experiments on selectively deuterium-labeled samples.

To a first approximation, we ignored the effect of internal motion on our estimates of the distances from phosphorus to the surrounding protons derived from the cycling experiment. However, this can be addressed using results from the molecular dynamics simulations. The molecular dynamics simulation trajectories obtained as described above were used to estimate dipolar order parameters S_d^2, which were in a range from 0.69 to 0.78 for the vectors connecting the phosphorus atoms to all four protons. Using a mean value of 0.74 in the required S_d^2 inserted on the left side of eq 2, we estimate a decrease in the predicted effective distance, from our combined data and simulation, of about 5% less than the preliminary average (Table 1), or $r_e = 2.29$ Å. The simulation also provides a theoretical set of phosphorus−proton distances. They are slightly longer than in the NMR structure (mean distances are 3.15, 2.87, 2.85, and 2.94 Å for H2″, H3′, H5′, and H5″, respectively), and the effective distance r_e derived from these values is 2.32 Å. (In the simulation, the effective distance for the GpG step is slightly higher than the others, at 2.34 Å; the remaining phosphates have an average of 2.30 Å.) In principle, both angle and distance fluctuations can influence r_e, but the distance fluctuations in the simulation are small enough to make this correction negligible, ca. 0.01 Å. Hence both the molecular dynamics simulation and the NMR structure (*44*) give effective distance sums (2.32 and 2.23 Å, respectively) that are very close to the corrected value of 2.29 Å that we extracted from the field-cycling data combined with the theoretical order parameters.

The coefficient C_L obtained from fitting the field dependence of R_1 to eq 1 provides an estimate of the CSA order parameter that does not have to be the same as that for dipolar relaxation. The CSA order parameters, S_c^2, for different phosphates in this concentrated octamer sample vary between 0.7 and 1 with low accuracy, but almost certainly reflecting a real variation among phosphodiester linkage dynamics, as previously reported (*7*). For this concentration of octamer, the S_c^2 is ∼1 for the ^{31}P resonance of the ApT and TpT phosphorus nuclei, which are in the middle of the duplex, as might be expected.

The high-field CSA relaxation variation is the low-frequency tail of a $\omega^2\tau$ curve with amplitude $(1 - S_c^2)$. Except for the ApT/TpT resonance, none of the other ^{31}P R_1 profiles could be well fit by an expression that included only dipolar and low-frequency CSA terms. In fact, at 14.0 and 17.6 T, where the high-frequency contribution is a substantial part of the relaxation rate, R_1 values of all but the central ApT/TpT resonances have substantially increased. Although there is significant error in extracting this parameter [since, for example, $(1 - S_c^2)$ is not precisely known], the average τ_{hf} is 146 ± 27 ps [with a range of 78−227 ps (Table 1)] for the 1.5 mM duplex sample.

The effect of possible magnetic ion impurities in the analysis above cannot be completely ruled out. We took typical precautions (*33*) to eliminate these impurities, and the consistency of the data between different samples argues against a large relaxation contribution from them. Over much of the low-field range that we study, magnetic moments of ions have longitudinal relaxation rates fast compared to the phosphorus angular nuclear resonance frequency, and only their time-average moment would be sensed by the nuclei (*45*). They would contribute a relaxation vs field contribution of a form similar to the low-field CSA relaxation, eq 1c. Magnetic impurities would be most likely to produce the largest errors at the intermediate fields around 4 T and would spuriously increase the CSA order parameters that we calculate from our data to be possibly greater than 1. Reassuringly, we do not find any such indications.

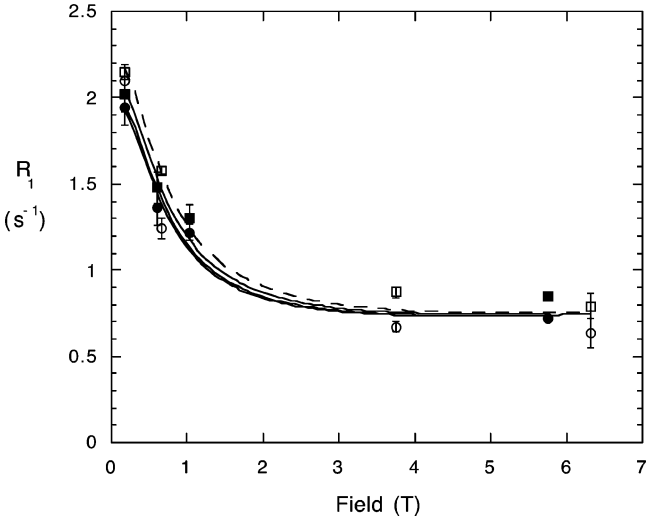

FIGURE 4: R_1 as a function of field for GpA (●) and ApA (■) in H_2O vs D_2O (same symbols, but not filled). The solid line is the calculated fit as described in the text. Note that there is no statistically significant difference for relaxation in the two solvents.

Field Dependence of ^{31}P R_1 for [d(GGAATTCC)]$_2$ in H_2O. It is possible that solvent molecules are close enough to contribute to the relaxation of the phosphorus nuclei in the DNA backbone. This can be probed by comparing R_1 as a function of field for the octamer dissolved in D_2O versus H_2O. If H_2O plays a significant role in the relaxation of the phosphorus nuclei, it should enhance $R(0)$. As shown in Figure 4, there is little difference in $R(0)$ for two such solutions at 1.5 mM duplex concentration (just the data for GpA and ApA are shown). Using average τ_r, C_L, and C_H values, $R(0)$ is 2.01 ± 0.06 s^{-1} for GpA in H_2O and 2.05 ± 0.10 s^{-1} in D_2O. Similarly, $R(0)$ is 2.14 ± 0.08 s^{-1} for ApA in H_2O and 2.27 ± 0.10 s^{-1} in D_2O. If one fits the data with only fixed τ_r and C_H, the $R(0)$ values are essentially the same. Thus, the protons responsible for ^{31}P relaxation in the octamer dissolved in low salt and no Mg^{2+} conditions do not include slowly exchanging (residence time >1 ns) water close to the phosphates.

Effect of Mg^{2+} on ^{31}P R_1 at Different Octamer Concentrations. Divalent cations bind strongly to nucleic acids and can affect their structure. This binding is generally explained as resulting from the strong interaction of the cations with the polyelectrolyte polymer, as a charge cloud in the spirit of Debye−Huckel theory (*46*), possibly with some degree of chelation (*47*). In the presence of excess Mg^{2+}, we find small chemical shift changes in a concentrated duplex sample, although CpC is still well separated from the other phosphates, and the phosphates in the center of the duplex are still likely to belong to the most upfield resonance. Since we could not assign resonances reliably in the presence of Mg^{2+}, we present only average behavior (Table 3).

Table 3: Effect of Mg^{2+} on Average Parameters Derived from the Field Dependence of ^{31}P R_1

duplex (mM)	Mg^{2+} (mM)	$R(0)$ (s^{-1})	r_e (Å)	τ_r (ns)	S_c^2	τ_{hf} (ps)
0.25	0	2.07 ± 0.08	2.38 ± 0.02	4.1 ± 0.2	0.66 ± 0.04	135[a]
0.25	5	2.06 ± 0.14	2.23 ± 0.07	2.8 ± 0.3	0.53 ± 0.09	135[a]
1.5	0	1.98 ± 0.08	2.41 ± 0.03	4.2 ± 0.3	0.80 ± 0.04	146 ± 27
1.5	50	3.55 ± 0.16	2.40 ± 0.05	7.4 ± 0.9	0.81 ± 0.10	124 ± 23

[a] Based on average C_H from analysis of 1.5 mM duplex $\pm$ Mg^{2+}.

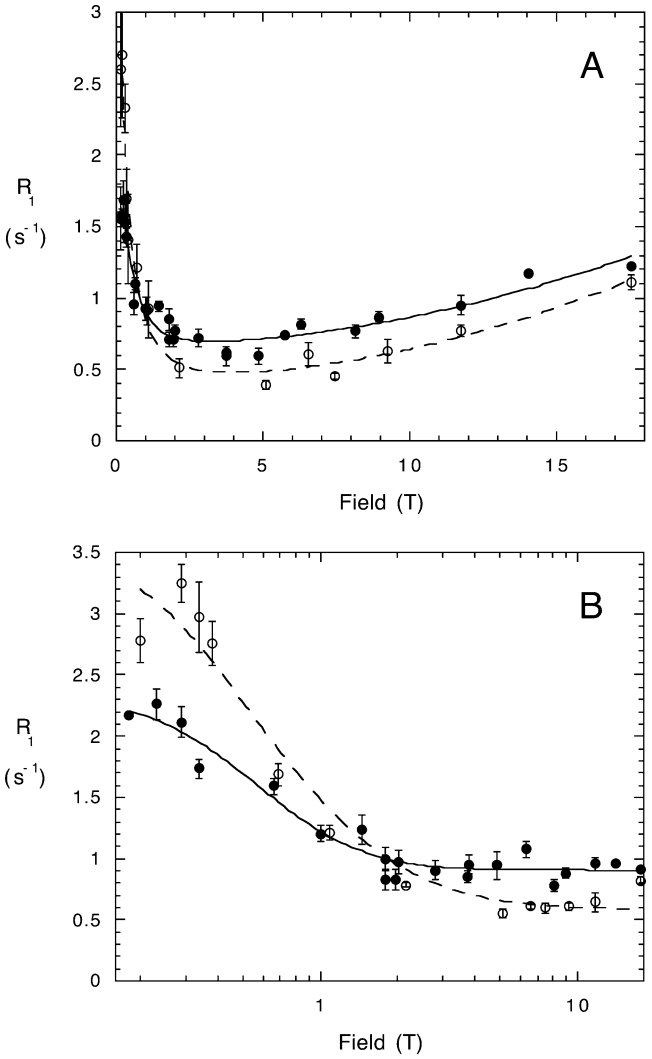

FIGURE 5: Field dependence of R_1 for (A) CpC and (B) ApT/TpT resonances (1.5 mM in duplex) in the absence (●) and presence (○) of 50 mM Mg^{2+}. The log of the field is plotted in (B) to emphasize the increase in $R(0)$ and the decrease in R_1 above 2 T caused by the addition of the Mg^{2+} to the octamer.

The field dependence of R_1 for the 1.5 mM (in duplex) octamer with 50 mM Mg^{2+} added shows a significantly different profile than that for the octamer in the absence of divalent cation (as an example, see Figure 5 for the effect of Mg^{2+} on CpC R_1). The relaxation rate in the midrange ($\sim$3 T) of the field decreased in amplitude, the high frequency increase was still observable, and $R(0)$ was higher than $R(0)$ for the octamer without Mg^{2+}. According to our analysis, the rotational correlation time increased to an average of 7.4 ± 0.9 ns, compared to an average value of 4.2 ns without Mg^{2+}. The average value of τ_{hf} was essentially the same as for the octamer in the absence of Mg^{2+} (average $\tau_{hf} = 124 \pm 23$ ps). The average CSA S_c^2 also showed little change (0.80 in the absence of Mg^{2+} at this concentration and 0.81 with Mg^{2+} added). A likely explanation for the increased τ_r is Mg^{2+}-induced oligomerization of the duplex at higher concentration due to increased electrostatic shielding.

To estimate whether aggregation of the octamer duplex is contributing to τ_r, we examined the field dependence of R_1 for a 6-fold diluted sample of the octamer, 0.25 mM in duplex (Figure 6). Since we did not have data for R_1 at 14.0 and 17.6 T and since Mg^{2+} had no significant effect on τ_{hf}, we used the average value (for the 1.5 mM duplex $\pm$ Mg^{2+}) of 135 ps for τ_{hf} in the fitting of the observed field dependence of R_1 for the more dilute samples. As can be seen in Table 3, the average τ_r extracted for all six resonances in the dilute sample without Mg^{2+} was 4.1 ns, essentially the same as for the Mg-free 1.5 mM duplex sample. Therefore, the octamer is not aggregating noticeably in the absence of Mg^{2+}. The average S_c^2 was slightly lower (0.66 ± 0.04) than in the more concentrated sample. Data were also acquired for the dilute octamer sample in the presence of excess Mg^{2+} (5 mM). Under these conditions, there was no longer an increase in τ_r induced by Mg^{2+}. Rather, τ_r decreased significantly (compare Tables 1 and 2) to about 2.8 ns. This is easily seen in Figure 6 at fields >2 T where R_1 for phosphates with added Mg^{2+} is uniformly higher than that in the absence of Mg^{2+}. A comparison of the S_c^2 values for the dilute octamer in the absence and presence of Mg^{2+} suggests that there is positional ordering in the duplex with the Mg^{2+} present (Figure 7). For phosphates in the middle of the octamer, S_c^2 extracted from these data for dilute duplex in the presence of excess Mg^{2+} was significantly greater than that for the duplex without Mg^{2+} at the same concentration. These results suggest that Mg^{2+} produces some aggregation at the higher concentration of the octamer but that at 6-fold lower concentration there is little or no aggregation, and Mg^{2+} condenses and orders the center of the molecule slightly.

Field Dependence of Proton R_1 for [d(GGAATTCC)]$_2$ in D_2O. High-resolution field cycling can also be used to measure proton R_1 values at different field strengths. We have measured proton R_1 in the octamer duplex (Figure 8) for a variety of protons (assignments from ref *48*) and found rapidly increasing relaxation rates at lower fields as expected, consistent with simple single- or dual-spin-flip dipolar relaxation by nearby protons. Because of the high signal-to-noise ratio, this relaxation can be estimated for fields where the rate is relatively high, even 30 s^{-1}, where spin diffusion cross-relaxation is relatively small. Such measurements are useful in evaluating proton-sourced NOE's but may also be useful in themselves for study of dynamics.

It is well-known that proton relaxation in macromolecules at high field (many tesla) is usually dominated by cross-

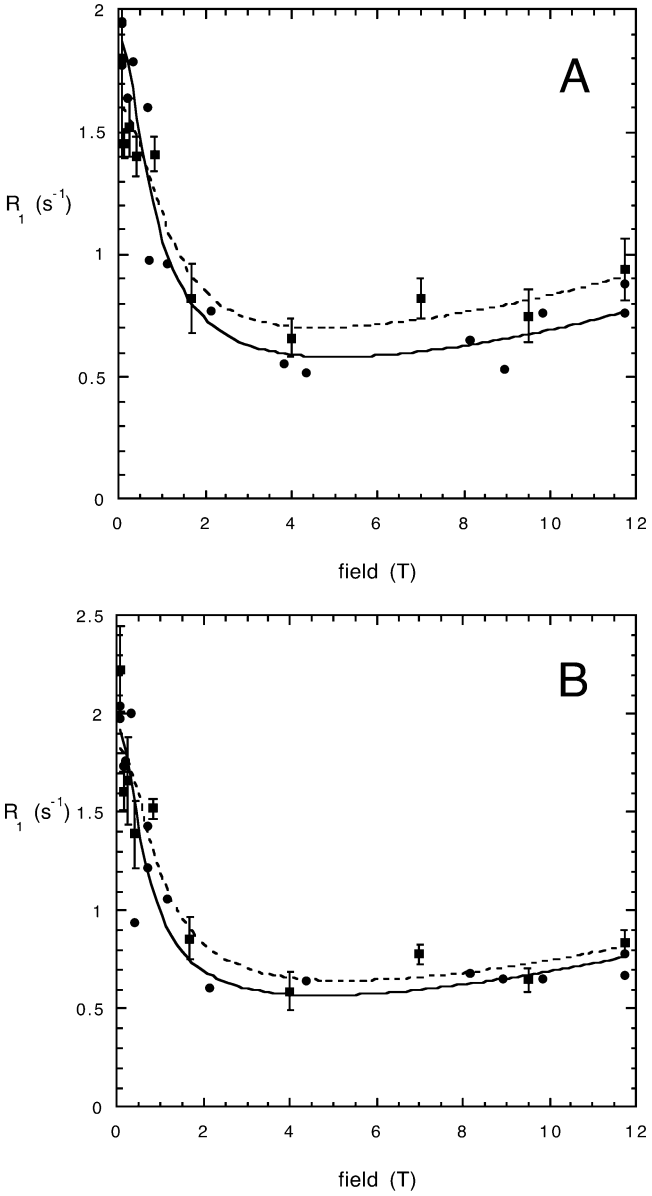

FIGURE 6: Field dependence of ^{31}P R_1 values for (A) CpC and (B) GpG in the octamer (0.25 mM in duplex) in the absence (●) and presence (■) of 5 mM Mg^{2+}. Error bars are shown for the relaxation rates determined in the presence of Mg^{2+}.

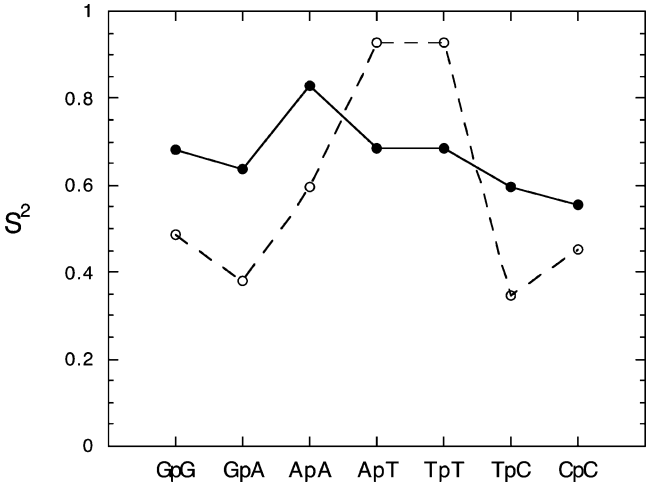

FIGURE 7: S_c^2 for 0.25 mM (in duplex) octamer solutions in the absence of Mg^{2+} (●) compared to S_c^2 for the sample with added Mg^{2+} (○).

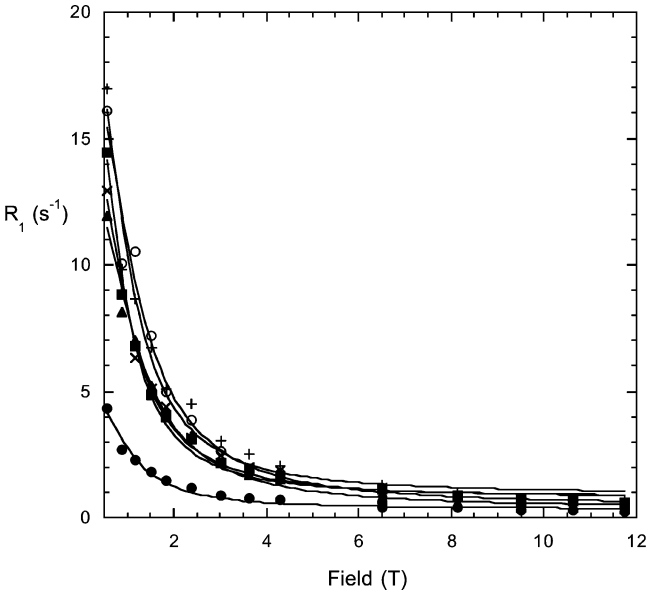

FIGURE 8: Field dependence of ^1H R_1 for selected protons of the octamer (1.5 mM duplex): (●) adenine C_2H; (■) cytidine C_6H; (▲) thymidine CH_3; (+) $C_{5'}H$; (○) average of the $C_{2'}H$ resonances.

relaxation between neighboring spins and diffusion of magnetization throughout many protons. Magnetization is generally assumed to be dissipated by the most rapidly relaxing spins, but because of spin diffusion the entire set (or large groups) of protons appear, in nonselective experiments such as ours, to relax at a low average rate (*49*). Our proton data at high field are consistent with this picture, with high-field rates in the range of $0.3-0.9\ s^{-1}$. Since the proton cross-relaxation rate with mutual opposite proton flips requires no energy, it is field independent, and this picture is expected to be valid down to fields where the so-called single- and double-quantum rates (that is, the single-flip and two-proton same-direction flip rates) start to become comparable to the field-independent zero-quantum (opposite two-proton flip or spin diffusion) rates. At these low fields, below about 4 T, individual protons or pairs of protons start to relax at individual rates, with protons that are nearest to other protons showing the most distinctly increasing rates. Again, this behavior is seen in Figure 8. However, the recovery behavior is not simple theoretically. Coupled relaxation equations for the proton magnetizations could be written and solved on a computer. Other experiments than simple relaxation could be performed, such as an NOE experiment. Such an experiment was already performed long ago by Kerwood and Bolton (*26*), and the expected reversal of NOE at low field was reported by them. Here we simply wished to exhibit the field dependence of the proton relaxation time, and we chose to fit the relaxation runs to simple exponential decays and treat the data as if there was only one simple relaxation spectrum with a single Lorentzian spectral density characterized by a single correlation time which we denote by τ_H (see the Materials and Methods section).

At low fields, dipolar relaxation for each proton should reflect the number and distance of nearby protons (Figure 8), as it does for ^{31}P. The relaxation rate $R(0)$ extrapolated to zero field is the smallest for the adenine C_2H's, as expected since these protons are relatively isolated from others, and

the rate is the largest for the ribose $C_2{}'H_2$ protons. $R(0)$ for other base or sugar protons and for the thymine methyl proteins are between those extreme values, depending as expected on proximity of other protons. The observation that different protons relax at different rates at low fields is in striking contrast to the high-field behavior where spin diffusion equalizes apparent R_1's.

After subtraction of the high-field constant rate, we can get a fairly good fit to a single apparent correlation time τ_H for all of the spins. Using the fit to a single Lorentzian and a constant term, the average τ_H is 4.2 ns, the same value as the rotational correlation time τ_r of 4.2 ns derived more rigorously from the ^{31}P data. Other protons display similar values. The parameter τ_H is expected to be approximately the same as the rotational correlation time, but at this point it is simply a phenomenological parameter that we will not attempt to interpret further.

Proton−proton NOE experiments with mixing intervals at low field could be uniquely interesting because they would have properties such as rotating-frame NOE experiments, but they may possibly be more useful than the rotating-frame method for observation of cross-relaxation over long distances.

Proton−Phosphorus Nuclear Overhauser Effect. The heteronuclear NOE is due to terms in the Solomon equations (*50*), which couple proton magnetization kinetically to the phosphorus magnetization. These terms are essentially the same in magnitude as the first and third terms of the right-hand side of eq 1b, but they have opposite sign. In the case of proton−proton NOE these terms cancel at a certain field, leading to the well-known null in NOE in this case (*26*). Because these kinetic terms increase at low fields, it is tempting to look for heteronuclear NOE using field cycling to increase the size of these terms relative to the competing relaxation terms including CSA relaxation. This remains an interesting possibility to apply to ^{13}C or ^{19}F, for example. Unfortunately, uniquely in the case of proton to ^{31}P NOE, the cancellation between these terms is nearly complete (within 10%) for all high fields because (i) the field is high enough so that the denominator terms, $(\gamma_H - \gamma_P)^2H^2\tau_r^2$ and $(\gamma_H + \gamma_P)^2H^2\tau_r^2$, are much greater than one, and (ii) these terms are nearly equal and opposite in sign for all such high fields. Being skeptical as always of formal relaxation theory, we did look for NOE at higher fields but found them only below about 1.5 T. At these fields the two terms above (zero and double quantum) become relatively different theoretically, and we did find a small NOE of ~2% (see the Materials and Methods section). The effect is extremely small because the proton relaxation rates are considerably shorter than the ^{31}P dipolar rates in general, including rates of those protons that would be most active in determining the NOE amplitude. The part of the proton magnetization labeled with the aid of phase cycling decays at a rate of around 10 s^{-1} (see Figure 8) during the NOE mixing time and also is lost to an appreciable extent during passage from the high field.

In view of this disappointment it is interesting to contemplate the extensive earlier relaxation and NOE measurements performed on longer duplex DNA fragments at fields in the range of 2 T or less [reviewed by James (*9*); see also ref *51*]. Those reported NOE's are presumably produced by what we term internal motions, including especially dynamic curving motions (writhing and twisting). These motions are not definable for a short octamer, or at least they are absorbed into the rotational diffusion that we consider in most of this paper. The writhing motions would probably have longer correlation times than the internal motions we deduce in the octamer. Presumably the ^{31}P relaxation rates we feature herein would all be decreased appreciably by the longer rotational correlation times in this older research, compared to our short octamer, or, in the case of the high-field CSA mechanism, reduced by the low fields used in the older work. These mechanisms would thus compete with any NOE buildup to a lesser extent than in the octamer. The transition rates for zero- and double-quantum rates probably did not cancel to such a large extent because of the low field used. Finally, the NOE is also easier to observe at fixed field because the protons can be steadily saturated in fixed field so that the effect is not decreased by the short proton T_1 as it is for our method.

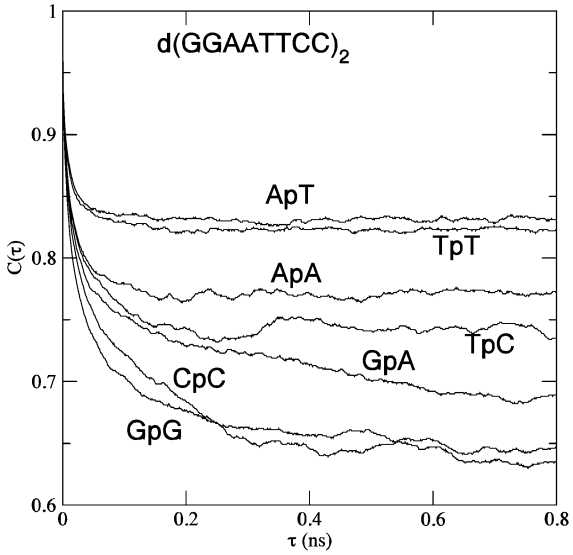

FIGURE 9: Time correlation functions from the MD simulation for the vector between P and the midpoint of O1P, O2P. Plots are given for just one of the two strands, but results from the other strand are similar.

Molecular Dynamics Simulation. The experimental relaxation rates are linear combinations of Fourier transforms of correlation functions of the appropriate interactions (*52*). In particular, the last term of eq 1c, with the substitution eq 4, comes from the assumption of an exponential correlation time of the CSA interaction. The molecular dynamics simulation was performed to test this assumption and to try to understand the experimentally determined correlation times and order parameters.

Figure 9 shows the correlation functions (after removing the overall rotation) for the vectors formed from the phosphorus nucleus ^{31}P to the middle point between O1P and O2P. For each curve, there is a rapid (<10 ps) decay, followed by a slow decay, reaching a plateau at times less than 0.5 ns, which is short compared to the 4 ns overall tumbling motion. Broadly similar behavior has been found for amide ^{15}N relaxation in proteins (*52*), but generally only very mobile regions in loops show the slow decays seen here, especially near the ends. The correlation times and order parameters are shown in Table 4. Since we have two identical sequences, the data shown in the table are the averaged values for the two chains.

Table 4: Order Parameters and Internal Decay Times (ps) from the MD Simulation

dinucleoside	S^2	τ_s	S_f^2	τ_f
GpG	0.61	244	0.76	9.5
GpA	0.70	244	0.78	10.0
ApA	0.77	33	0.87	2.7
ApT	0.83	25	0.90	1.6
TpT	0.82	61	0.87	3.2
TpC	0.76	83	0.84	4.7
CpC	0.65	160	0.78	8.4
av	0.73	121	0.83	5.7

The fast correlation times τ_f are less than 10 ps, which reflect mostly local vibrational motion. The slow correlation times τ_s are in the range of 25−244 ps, which reflect other internal motion such as torsional librations and more extended motions. These correlation times are shorter in the middle of the octamer and become longer toward the ends. We can also see higher order parameters in the middle of the octamer, becoming lower toward the ends. These parameters indicate that the middle part of the octamer is somewhat more rigid than are the ends, as expected.

Compared with the field-cycling NMR data shown in Table 1, we see good agreement for the average S^2 and τ_s values. The molecular dynamics results show higher order parameters and shorter time constants in the middle of the helix compared to the ends, as expected; this is broadly the trend seen in the data extracted from the NMR data for the 1.5 mM duplex as well. In the NMR experiment, the resonance peaks of ApT and TpT are overlapped, but the simulation results predict that the corresponding time correlation functions are very similar.

Although the order parameters extracted using eq 7 provide a good description of the computed time-correlation functions, there is some uncertainty involved in comparing these to the S_c^2 values in Table 1. This is because we do not know the value of σ^2 that is appropriate in the absence of any motional averaging. The solid-state value we have used (160 ppm) presumably incorporates some of the same reduction (from its zero-motion limit) due to local vibrational averaging that is seen at very short times in the computed correlation functions in Figure 9. An analogous situation is well-known for dipolar couplings (*53*), but we do not know a priori how great this local vibrational reduction is in the solid-state experiments. Analysis of protein simulations suggests that these intrinsic vibrational corrections (which are assumed to be the same in model solid-state peptides and in proteins) lead to decays with time constants of less than 1 ps. Our computed time-correlation functions for all phosphates decay to 0.92 ± 0.01 at $\tau = 1$ ps, suggesting that this decay is an intrinsic local feature of the phosphodiester group. If this motion is also present in the solid-state experiment, then it should be removed from the computed order parameters when making comparisons to S_c^2. In this simple model (which needs to be tested with further experiments and calculations), one should compare S_c^2 with the computed values of $S^2/0.92$; such a correction would make the average computed order parameter be 0.79, which is close to the field-cycling result from Table 1.

To further look at the internal motion, we calculated time series of the six torsion angles of the backbone of the octamer. In the middle of the backbone, the time-averaged

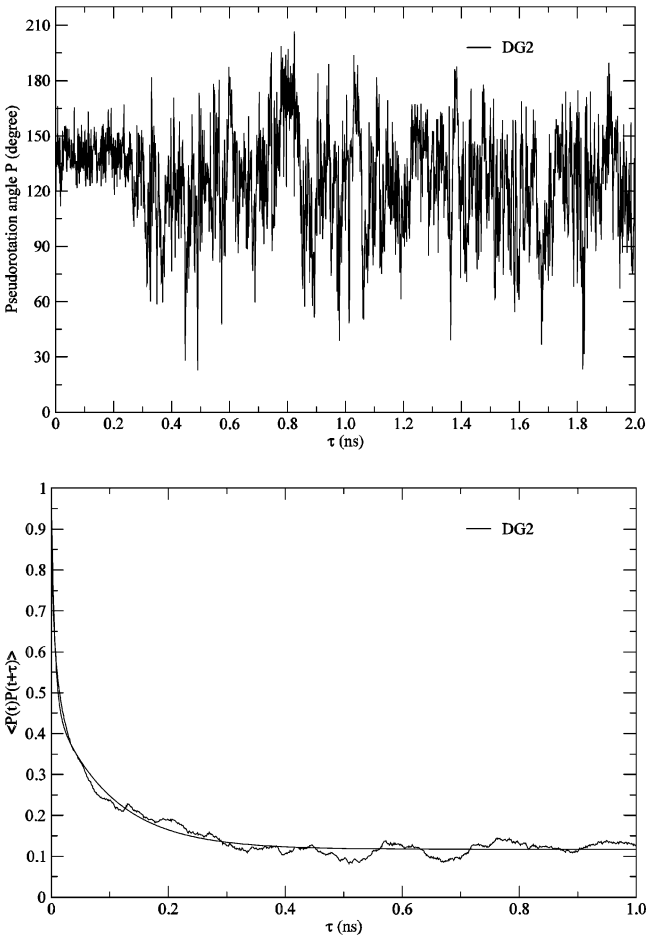

FIGURE 10: (Top) Time dependence of the sugar pucker for G_2 showing the first two nanoseconds only. (Bottom) Autocorrelation function for the top time series, computed for the full 28 ns trajectory. The smooth line shows a fit to a short exponential, not related to our discussion, and a longer exponential with a time constant of 99 ps. The slow fluctuations giving rise to this feature can be seen, for example, in the regions near 0.8 ns, and 1.7 ns, in the top plot.

values for α, *β*, *γ*, *δ*, *ϵ*, and *ζ* are about −60°, 180°, 60°, 110°, 180°, and −90°, respectively. *δ* (which reports the sugar pucker) has the largest fluctuation, from 70° to 150°, and the time constants for decay of fluctuations in *δ* back to average values are on the order of 50−100 ps; even longer values are seen for the sugar pucker pseudorotation angle itself, especially near the ends of the chain. By contrast, time decay constants for other backbone torsions are shorter. This suggests that the slower motions picked up by ^{31}P relaxation are related to fluctuations in the sugar pucker pseudorotation. Note the fluctuations involved here are not primarily between the C2′ endo and C3′ endo (or "north" and "south") local minima; rather they are within the general south category (or B-form DNA) sugar pucker region between about 120° and 180°. For example, Figure 10 (top) shows the first two nanoseconds of the time course of the sugar pucker angle for the G_2 nucleotide. Even within the B-form sugar pucker region, there are large and relatively slow fluctuations. The time decay of these fluctuations is closely fit by an exponential with a time constant of 99 ps (Figure 10, bottom). The mean decay time for fluctuations in pseudorotation pucker for all sugars is 75 ps. Other analyses can be used to help to identify collective motions that contribute to particular

relaxation processes (*54*), and these will be pursued elsewhere.

DISCUSSION

Field-cycling NMR dates back to R. V. Pound's experiments in 1952, hand-shuttling a sample to nearly zero field (*15*), which raised questions for the first time about nuclear spin thermodynamics. Field-cycling studies of water relaxation has been used to study solvent interactions in a wide variety of systems [for example, see work by Dr. R. G. Bryant and co-workers (*30*, *55*, *56*)]. The present version of this experiment uses sample shuttling to change the field for evolution of the spin system but also utilizes the signal at high field for readout to obtain high-resolution information. It is particularly useful for nuclei without nearby protons whose relaxation is dominated by mechanisms other than dipolar interactions at high fields. Since phosphate esters are key components of many macromolecules (nucleic acids, phosphoproteins, phospholipids) and small biological molecules (e.g., sugar phosphates, ATP, glycerol phosphate), ^{31}P nuclei are good targets for field cycling. Analysis at high field provides the chemical shift dispersion (and sensitivity) needed to follow distinct phosphates in macromolecules.

The previous proton and ^{31}P study of a DNA dodecamer by Lane et al. (*7*) reached conclusions in excellent agreement with ours, considering that measurements at only two fields were used by them. The correlation time was estimated to be 3.8 ns, and the effective distance from protons to phosphorus was 2.2 Å. CSA order parameters were found to differ between linkages and were in approximately the same range as ours. The high-field CSA relaxation was not elucidated. Even if it had been deduced by measurements at multiple high fields, a precise and convincing deduction of the relaxation parameters would have been impossible without lower field data.

Using a standard theoretical framework for interpreting the field dependence of ^{31}P R_1, we can extract several useful descriptive parameters: τ_r, the molecular correlation time; r_e, the effective distance of nearby protons to the phosphorus; S_c^2, the chemical shift anisotropy order parameter; and τ_{hf}, a correlation time for faster motions. Analysis of the field dependence of R_1 over a large field range may sometimes be superior to other methods for estimating rotational correlation times because it is based on observations at many frequencies, rather than an analysis of rate ratios such as an R_1/R_2 ratio that could be affected by exchange of the nuclei between different environments, and other unknowns. The value of τ_r can almost be directly read from the inverse of the half-width of the low-frequency bump in the R_1 plot in our data. The geometrical distance average r_e that we extract from our data agrees with the same average from the published dodecamer structure (*44*) within 3%, after we corrected our analysis slightly using proton−phosphorus order parameters extracted from the simulation.

The increased τ_r for the concentrated octamer solution in the presence of Mg^{2+} is consistent with aggregation of this species under these conditions. Theories and experiments have shown that counterion-induced aggregation of longer DNA molecules forms condensed rodlike structures (*57*). While there is little in the literature with reference to cation-induced aggregation of smaller oligonucleotides, the high Mg^{2+} concentration used in these experiments as well as high DNA concentration clearly causes some degree of aggregation.

The CSA S_c^2 extracted for each ^{31}P from our field-cycling experiments is not easily obtained by other methods. The ability to measure this parameter, and to monitor changes when different solutes or ligands are added, should have a wide range of uses in physical biochemistry. In the case of the dilute DNA octamer under conditions where aggregation of the DNA does not occur, S_c^2 was significantly increased in the middle of the molecule when Mg^{2+} was added into the system. Similar extrapolated S_c^2 values, but for DNA duplexes where there are specific interactions with small molecules (intercalators, groove binders, etc.) or where there are base mismatches, could be very useful in characterizing nucleic acid dynamics.

One of the surprises in the initial data set for the DNA octamer was the need to include a high-field internal motion CSA component for all but the ApT/TpT resonance. Although a precise understanding of this parameter in terms of specific motions is not yet available, it is a second time constant that can be used to characterize phosphate dynamics under a wide variety of conditions. For example, it remains to be seen if τ_{hf} values ∼100−200 ps occur for other phosphodiesters as well as for the phosphates in DNA. The molecular dynamics simulation shows an average time scale for motion of the phosphate internal motion of 121 ps and an average corrected squared order parameter of 0.79, in good agreement with parameters extracted from the high-resolution cycling observations. The simulation also indicates that the internal motion reported by the relaxation at high field is associated mainly with dynamics of changes in sugar puckering.

If the underlying biophysical phenomena are still of interest, it would be worth returning to measurements on longer DNA duplex samples (*9*) using field cycling. The longer DNA duplexes differ from the octamer in that a part of the internal motion should have a much longer correlation time than the ∼0.1 ns internal correlation time that dominates our study, whereas the overall rotational correlation time will be longer than that of the octamer. These longer DNAs could, therefore, have interesting dispersion in their relaxation rate curves below the range of 0.05 T. In our ongoing study of ^{31}P relaxation in phospholipid vesicles (M. F. Roberts and A. G. Redfield, unpublished results), we have indeed seen low-frequency dispersions below 0.05 T, presumably associated with processes such as overall tumbling of vesicles and micelles at rates of the order 10^6 s^{-1}. We will present these results elsewhere.

We hope that observations such as these, on more interesting nucleic acids, can be useful in interpreting the dynamics of their parts in mechanistically useful ways. Observation of cross-correlation effects between dipolar and CSA relaxation on R_1 is another exciting possibility to be explored (*13*). At around 2 T the rate for conversion of double- to single-quantum conversion is increased by an increase in the relevant spectral density (*13*), and the competing total R_1 rates for phosphorus and protons remain low (data herein), possibly facilitating such measurements.

High-resolution field cycling should also be informative for certain ^{13}C nuclei. Field-dependent phenomena similar to what we have seen with ^{31}P should be observable for ^{13}C′

(carboxyl, carbonyl ^{13}C nuclei) which have no attached protons, especially in highly deuterated proteins. In particular, observation of an NOE at higher fields, where the longer proton T_1 will facilitate selective NOE, may be possible for $^{13}C'$ spins which do not have the annoying near cancellation of NOE rates for opposite mutual flips compared to same-direction flips, which ^{31}P has at higher field, as discussed earlier.

ACKNOWLEDGMENT

The present work was greatly influenced by contacts of A. G. Redfield with Dr. Seymour Koenig, over many years at the IBM Watson Laboratory (may it rest in peace) at Columbia University. We thank Dr. Holger Gohlke for assistance with the calculations and Dr. Jerome Boisbouvier, NIH, for calculating the average we call r_e in the DNA dodecamer and for sending a preprint on ^{13}C relaxation, and we thank him and Dr. Tom James for useful suggestions.

REFERENCES

1. Clore, G. M., Murphy, E. C., Gronenborn, A. M., and Bax, A. (1998) Determination of three-bond $^1H3'$-^{31}P couplings in nucleic acids and protein nucleic acid complexes by quantitative J correlation spectroscopy, *J. Magn. Reson. 134*, 164−167.
2. Yang, J., McAteer, K., Silks, L. A., Wu, R., Isern, N. G., Unkefer, C. J., and Kennedy, M. A. (2000) A comprehensive approach for accurate measurement of proton−proton coupling constants in the sugar ring of DNA, *J. Magn. Reson. 146*, 260−276.
3. Wu, Z., Tjandra, N., and Bax, A. (2001) ^{31}P chemical shift anisotropy as an aid in determining nucleic acid structure in liquid crystals, *J. Am. Chem. Soc. 123*, 3617−3618.
4. Wu, Z., Tjandra, N., and Bax, A. (2001) Measurement of $^1H3'$-^{31}P dipolar couplings in a DNA oligonucleotide by constant-time NOESY difference spectroscopy, *J. Biomol. NMR 19*, 367−370.
5. Majumdar, A., and Patel, D. J. (2002) Identifying hydrogen bond alignments in multistranded DNA architectures by NMR, *Acc. Chem. Res. 35*, 1−11.
6. Yan, J., Corpora, T., Pradhan, P., and Bushweller, J. H. (2002) MQ-HCN-based pulse sequences for the measurement of $^{13}C1'$-$^1H1'$, $^{13}C1'$-^{15}N, $^1H1'$-^{15}N, $^{13}C1'$-$^{13}C2'$, $^1H1'$-$^{13}C2'$, $^{13}C6/8$-$^1H6/8$, $^{13}C6/8$-^{15}N, $^1H6/8$-^{15}N, $^{13}C6$-$^{13}C5$, $^1H6$-$^{13}C5$ dipolar couplings in ^{13}C, ^{15}N-labeled DNA (and RNA), *J. Biomol. NMR 22*, 9−20.
7. Lane, A. N., Jenkins, T. C., Brown, T., and Neidle, S. (1991) Interaction of berenil with the EcoRI dodecamer d(CGCGAATTCGCG)$_2$ in solution studied by NMR, *Biochemistry 30*, 1372−1385.
8. Keepers, J. W., and James, T. L. (1982) Models for DNA backbone motions—an interpretation of NMR relaxation experiments, *J. Am. Chem. Soc. 104*, 929−939.
9. James, T. L. (1984) Relaxation behavior of nucleic acids: dynamics and structure, in *Phosphorus-31 NMR Principles and Applications* (Gorenstein, D., Ed.) pp 349−400, Academic Press, New York.
10. Hart, P. A. (1984) Phosphorus relaxation methods: conformation and dynamics of nucleic acids and phosphoproteins, in *Phosphorus-31 NMR Principles and Applications* (Gorenstein, D., Ed.) pp 317−347, Academic Press, New York.
11. Boisbouvier, J., Wu, Z., Ono, A., Kainosho, M., and Bax, A. (2003) Rotational diffusion tensor of nucleic acids from ^{13}C NMR relaxation, *J. Biomol. NMR 27*, 133−142.
12. Spielmann, H. P. (1998) Dynamics in psoralen-damaged DNA by ^1H-detected natural abundance ^{13}C NMR spectroscopy, *Biochemistry 37*, 5426−5428.
13. Kojima, C., Ono, A., Kainosho, M., and James, T. L. (1999) Quantitative measurement of transverse and longitudinal cross-correlation between ^{13}C-^1H dipolar interaction and ^{13}C chemical shift anisotropy: Application to a ^{13}C-labeled DNA duplex, *J. Magn. Reson. 136*, 169−175.
14. Redfield, A. G. (2003) Shuttling device for high-resolution measurements of relaxation and related phenomena in solution at low field, using a shared commercial 500 MHz NMR instrument, *Magn. Reson. Chem. 41*, 753−768.
15. Pound R. V. (1951) Nuclear spin relaxation time in a single crystal of LiF, *Phys. Rev. 81*, 156.
16. Noack, F. (1986) Field-cycling spectroscopy: principles and applications, *Prog. NMR Spectrosc. 18*, 171−276.
17. Bertini, I., and Luchinat, C. (1986) *Paramagnetic Molecules in Biological Systems*, Benjamin/Cummings, Menlo Park, CA.
18. Koenig, S. H. (1995) The dynamics of water in biological systems, in *Encyclopedia of NMR* (Grant, D. M., and Harris, R. K., Eds.) pp 1817−1830, John Wiley, New York.
19. Job, C., Zajicek, J., and Brown, M. F. (1996) Fast field-cycling nuclear magnetic resonance spectrometer, *Rev. Sci. Instrum. 67*, 2113−2122.
20. Redfield, A. G. (1996) Field cycling NMR applied to macromolecular structure and dynamics, in *NMR as a Structural Tool for Macromolecules* (Rao, B. D. N., and Kemple, M. D., Eds.) pp 123−132, Plenum Press, New York.
21. Kimmich, R. (1997) *NMR: Tomography, Diffusometry, Relaxometry*, Springer-Verlag, Heidelberg.
22. Mandel, A. M., Akke, M., and Palmer, A. G., III (1995) Backbone dynamics of *Escherichia coli* ribonuclease HI: correlations with structure and function in an active enzyme, *J. Mol. Biol. 246*, 144−163.
23. Brown, M. F., Thurmond, R. L., Dodd, S. W., Otten, D., and Beyer, K. (2002) Elastic deformation of membrane bilayers probed by deuterium NMR relaxation, *J. Am. Chem. Soc. 124*, 8471−8484.
24. Halle, B., and Denisov, V. P. (2001) Magnetic relaxation dispersion studies of biomolecular solutions, *Methods Enzymol. 338* (Part A), 178−201.
25. Strombotne, R. L., and Hahn, E. L. (1964) Longitudinal nuclear spin−spin relaxation, *Phys. Rev. 133*, A1616−A1629.
26. Kerwood, D. J., and Bolton, P. H. (1986) Low field NMR, *J. Magn. Reson. 68*, 142−146.
27. Stob, S., Kemmink, J., and Kaptein, R. (1989) Intramolecular electron-transfer in flavin adenine-dinucleotide—photochemically induced dynamic nuclear-polarization study at high and low magnetic fields, *J. Am. Chem. Soc. 111*, 7036−7042.
28. Emsley, L., and Pines, A. (1993) Lectures on Pulsed NMR, in *Nuclear Magnetic Double Resonance* (Maraviglia, B., Ed.) 2nd ed., North-Holland, Amsterdam.
29. Grosse, S., Gubaydullin, H., Scheelken, H., Vieth, H.-M., and Yurkovskaya, A. V. (1999) Field cycling by fast NMR probe transfer: Design and application in field-dependent CIDNP experiments, *Appl. Magn. Reson. 17*, 211−225.
30. Wagner, S., Dinesen, T. R., Rayner, T., and Bryant, R. G. (1999) High-resolution magnetic relaxation dispersion measurements of solute spin probes using a dual-magnet system, *J. Magn. Reson. 140*, 172−178.
31. Connolly, B. A., and Eckstein, F. (1984) Assignment of resonances in the ^{31}P NMR spectrum of d(GGAATTCC) by regiospecific labeling with ^{17}O, *Biochemistry 23*, 5523−5527.
32. Sambrook, J., Fritsch, E. F., and Maniatis, T. (1989) *Molecular Cloning*, 2nd ed., pp E37−E38, Cold Spring Harbor Press, Cold Spring Harbor, NY.
33. Hart, P. A. (1978) Conformation of mononucleotides and dinucleoside monophosphates. P[H] and H[H] nuclear Overhauser effects, *Biophys. J. 24*, 833−848.
34. Shindo, H. (1984) Solid-state phosphorus-31 NMR: Theory and application to nucleic acids, in *Phosphorus-31 NMR Principles and Applications* (Gorenstein, D., Ed.) pp 401−422, Academic Press, New York.
35. Herzfeld, J., Griffin, R. G., and Haberkorn, R. A. (1978) Phosphorus-31 chemical-shift tensors in barium diethyl phosphate and urea-phosphoric acid: model compounds for phospholipid headgroup studies, *Biochemistry 17*, 2711−2718.
36. Lipari, G., and Szabo, A. (1982) Model-free approach to the interpretation of nuclear magnetic resonance relaxation in macromolecules. 1. Theory and range of validity, *J. Am. Chem. Soc. 104*, 4546−4559.
37. Case, D. A., Pearlman, D. A., Caldwell, J. W., Cheatham, T. E., III, Wang, J., Ross, W. S., Simmerling, C. L., Darden, T. A., Merz, K. M., Stanton, R. V., Cheng, A. L., Vincent, J. J., Crowley, M., Tsui, V., Gohlke, H., Radmer, R. J., Duan, Y., Pitera, J., Massova, I., Seibel, G. L., Singh, U. C., Weiner, P. K., and Kollman, P. A. (2002) *AMBER 7*, University of California, San Francisco.
38. Cornell, W. D., Cieplak, P., Bayly, C. I., Gould, I. R., Merz, K. M., Jr., Ferguson, D. M., Spellmeyer, D. C., Fox, T., Caldwell, J. W., and Kollman, P. A. (1995) A second generation force field for the simulation of proteins, nucleic acids, and organic molecules, *J. Am. Chem. Soc. 117*, 5179−5197.

39. Jorgensen, W. L., Chandrasekhar, J., Madura, J. D., Impey, R. W., and Klein, M. L. (1983) Comparison of simple potential functions for simulating liquid water, *J. Chem. Phys. 79*, 926−935.
40. Darden, T., York, D., and Pedersen, L. (1993) Particle mesh Ewald: An *N*·log(*N*) method for Ewald sums in large systems, *J. Chem. Phys. 98*, 10089−10092.
41. Ryckaert, J. P., Ciccotti, G., and Berendsen, H. J. C. (1977) Numerical-integration of Cartesian equations of motion of a system with constraints—molecular-dynamics of *n*-alkanes, *J. Comput. Phys. 23*, 327−341.
42. Clore, G. M., Szabo, A., Bax, A., Kay, L. E., Driscoll, P. C., and Gronenborn, A. M. (1990) Deviations from the simple two parameter model free approach to the interpretation of ^{15}N nuclear magnetic relaxation of proteins, *J. Am. Chem. Soc. 112*, 4989−4990.
43. Williamson, J. R., and Boxer, S. G. (1989) Multinuclear NMR studies of DNA hairpins. 1. Structure and dynamics of d(CGCGTTGTTCGCG), *Biochemistry 28*, 2819−2831.
44. Wu, Z., Delaglio, F., Tjandra, N., Zhurkin, V. B., and Bax, A. (2003) Overall structure and sugar dynamics of a DNA dodecamer from homo- and heteronuclear dipolar couplings and ^{31}P chemical shift anisotropy, *J. Biol. NMR 26*, 297−315.
45. Gueron, M. (1975) Nuclear-relaxation in macromolecules by paramagnetic ions—novel mechanism, *J. Magn. Reson. 19*, 58−66.
46. Gueron, M., Demaret, J.-Ph., and Filoche, M. (2000) A unified theory of the B-Z transition of DNA in high and low concentrations of multivalent ions, *Biophys. J.* 1070−1083.
47. Manning, G. D. (1978) The molecular theory of polyelectrolyte solutions with applications to the electrostatic properties of polynucleotides, *Q. Rev. Biophys. 11*, 179−246.
48. Patel, D. J., Shapiro, L., and Hare, D. (1987) Nuclear magnetic resonance and distance geometry studies of DNA structures in solution, *Q. Rev. Biophys. 20*, 35−112.
49. Kalk, A., and Berendsen, H. J. C. (1976) Proton magnetic-relaxation and spin diffusion in proteins, *J. Magn. Reson. 24*, 343−366.
50. Neuhaus, D., and Williamson, M. (1989) *The Nuclear Overhauser Effect*, VCH Publishers, New York.
51. Odahara, T., Nishimoto, S., Katsutani, N., Kyogoku, Y., Morimoto, Y., Matsuhiro, A., and Akutsu, H. (1994) Dynamic properties of nnucleic-acids in biosupramolecular systems, as studied by ^{31}P NMR, *J. Biochem. (Tokyo) 115*, 270−278.
52. Case, D. A. (2002) Molecular dynamics and NMR spin relaxation in proteins, *Acc. Chem. Res. 35*, 325−331.
53. Case, D. A. (1999) Calculations of NMR dipolar coupling strengths in model peptides, *J. Biomol. NMR 15*, 95−102.
54. Prompers, J. J., and Brüschweiler, R. (2001) Reorientational eigenmode dynamics: A combined MD/NMR relaxation analysis method for flexible parts in globular proteins, *J. Am. Chem. Soc. 123*, 7305−7313.
55. Godefroy, S., Korb, J. P., Fleury, M., and Bryant, R. G. (2001) New ways of probing surface nuclear relaxation and microdynamics of water and oil in porous media, *Magn. Reson. Imaging 19*, 517−519.
56. Korb, J. P., and Bryant, R. G. (2002) The physical basis for the magnetic field dependence of proton spin−lattice relaxation rates in proteins, *Magn. Reson. Med. 48*, 21−26.
57. Tang, J. X., Wong, S., Tran, P. T., and Janmey, P. A. (1996) Counterion induced bundle formation of rodlike polyelectrolytes, *Ber. Bunsen-Ges. Phys. Chem. 100*, 796−806.

BI035979Q